A Cadmium-Free Cu_2ZnSnS_4/ZnO Heterojunction Solar Cell Prepared by Practicable Processes

Myo Than Htay*, Yoshio Hashimoto, Noritaka Momose[1], Kouichi Sasaki, Hiroshi Ishiguchi, Shigeo Igarashi, Kazuki Sakurai, and Kentaro Ito

Department of Electrical and Electronic Engineering, Faculty of Engineering, Shinshu University, 4-17-1 Wakasato, Nagano 380-8553, Japan
[1]*Department of Electrical and Electronic Engineering, Nagano National College of Technology, 716 Tokuma, Nagano 381-8550, Japan*

A Cadmium-free Cu_2ZnSnS_4/ZnO hetrojunction solar cell with conversion efficiency of 4.29% has been obtained. The Cu_2ZnSnS_4 absorber film was formed utilizing sulfurization of laminated metallic precursors, and the ZnO buffer layer was then deposited on it by ultrasonic spray pyrolysis. In comparison with a conventional Cu_2ZnSnS_4/CdS hetrojunction solar cell, the open circuit voltage as well as the relative quantum efficiency at the short-wavelength regions was increased. The in-plane homogeneity of p-n junction was improved by depositing the ZnO layer on Cu_2ZnSnS_4 film via ultrasonic spray pyrolysis.

1. Introduction

A p-type quaternary compound, Cu_2ZnSnS_4 (CZTS), is one of the promising candidate semiconductors for photovoltaic applications because it not only consists of abundant elements, but has an optimum band gap of about 1.5 eV with a high absorption coefficient of the order of 10^4 cm^{-1}.[1–3] In addition to these properties, its toxicity is relatively low compared to the compounds containing selenium such as $Cu_2Zn_{1-x}Cd_xSn(Se_{1-y}S_y)_4$, $Cu_2ZnSn(Se,S)_4$, $Cu(In,Ga)Se_2$, and CdTe so that it is very attractive as a light absorber material for solar cells.[4–8] Several research efforts have recently been made on the CZTS-based solar cells since Katagiri *et al.* reported a CZTS/CdS hetrojunction solar cell with 6.77%.[9–15] However, an intensive usage of highly toxic cadmium compound such as CdS, prohibited by the RoHS (Restriction of the use of certain Hazardous Substances in electrical and electronic equipment) regulations, is a drawback and an alternative material is desirable to realize a more environment-friendly device.

In this paper, we introduce a practicable technique to fabricate a Cd-free heterojunction solar cell based on the CZTS absorber. Precursors that composed of alternatively laminated Cu, Zn, Sn

*E-mail address: myoth@shinshu-u.ac.jp

metal layers were used in synthesizing the CZTS thin films via sulfurization under elemental sulfur vapor. The formation of a CZTS/ZnO hetrojunction was realized by depositing a ZnO layer on the CZTS film utilizing ultrasonic-spray pyrolysis (USP).[16] Using ZnO (the band gap: 3.37 eV at room temperature[17]) as a buffer layer instead of CdS (the band gap: 2.42 eV at room temperature[18]), an enhancement of light transmittance in the shorter wavelength regions was achieved. The deposition of the ZnO layer by the USP technique has advantages over chemical bath deposition (CBD) technique, since it is superior in obtaining a single phase high quality ZnO layer directly on a substrate without any post-annealing process: the former process is free from the formation of a hydroxyl phase such as $Zn(OH)_2$ that degrade the quality of ZnO. Since the thin film growth process by USP is quite similar to that of chemical vapor deposition (CVD), the surface reaction of the present technique is favorable to obtain good step coverage. In other words, the film is deposited indiscretely on the substrate independent of its surface morphology, resulting in an enhancement of in-plane homogeneity of the CZTS/ZnO hetrojunction without damaging the CZTS film.

2. Experimental Methods

CZTS absorbers were grown on scraped soda-lime glass (SLG) substrates with a sputter-deposited Mo layer as follows. A laminated precursor composed of Cu, Zn, and Sn metal layers was annealed under ambient sulfur vapor in a closed glass tube heated with an infrared furnace. The detail of the reaction furnace was described elsewhere.[19] The sulfur vapor pressure was adjusted by the enclosed amount of elemental sulfur powder and the temperature inside the reaction tube based on the ideal gas law. Compositional control was achieved by varying the thickness ratio of laminated metal layers. A schematic of the laminated precursor was shown in Fig. 1. Here, a total of nine thin metal layers were stacked in the order as shown in the figure. The Cu and Sn layers were separated by Zn layers. On the top layer, a Zn metal was coated. A total thickness of precursor was adjusted to about 1 μm. To implement the CZTS/ZnO hetrojunction, the deposition of undoped ZnO layer on the CZTS absorber film was carried out by using original USP technique, and the details of the USP system were reported in our previous work.[16] Zinc acetate di-hydrate was used as a source species for zinc, and de-ionized water which also acts as a solvent for the precursor solution was used as an oxygen source. In this technique, resistivity of ZnO films was controlled by adjusting the deposition temperature and flow rate of precursor mist. After the formation of CZTS/ZnO junction, a ZnO:Al transparent conductive layer was deposited by radio frequency magnetron sputtering to complete a SLG/Mo/CZTS/ZnO/ZnO:Al cell structure. No antireflection coating was applied.

Current-voltage (*J*-*V*) characteristics of the devices were measured under AM 1.5 spectrum of 1 kW/m^2 irradiance. For evaluating the external quantum efficiency (*QE*) of the cell, a spectrometer

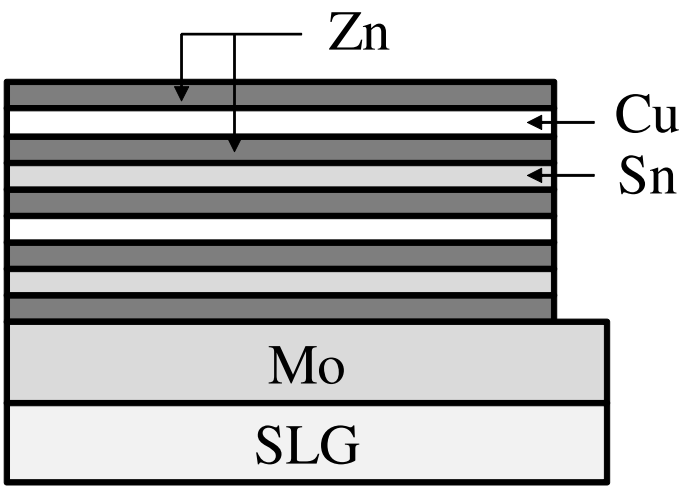

Fig. 1. A schematic of a laminated metallic precursor of CZTS film.

(Shimadzu UV-3100) was used. For comparison, a conventional CZTS/CdS hetrojunction cell was used, in which a CdS layer was prepared by a CBD method. A field emission scanning electron microscope (FE-SEM; Hitachi S-4100) was used to investigate the surface morphology of the samples. The compositional analysis was conducted by using electron probe microanalysis (EPMA; Shimadu EPMA-1610). A transmission electron microscopy (TEM; JEOL JEM-2010, LaB_6 cathode) was carried out at an acceleration voltage of 200 kV to study the cross sectional structure of the cells. To evaluate the resistivity of ZnO films, the sample films were deposited directly on the glass substrates and a four probe method was applied.

3. Results and Discussion

3.1 Effect due to the properties of ZnO buffer layer

Figure 2(a) shows the surface morphology of a CZTS absorber film which was used for preparing the solar cells in this work. The film was obtained by sulfurizing of a laminated metallic precursor under sulfur vapor pressure of 0.27 atm at 550 ˚C for 15 min. The compositional ratios of the film were Cu/(Zn + Sn) = 0.68, Cu/2Zn = 0.54, Cu/2Sn = 0.92, Zn/Sn = 1.71, and (Cu + Zn + Sn)/S = 0.98, respectively with 5% variation. It is revealed by the XRD pattern shown in Fig. 2(c) that a polycrystalline CZTS film was grown while containing SnS_2 crystallites as a minority phase. The surface morphology of the CZTS film after the deposition of a ZnO buffer layer by USP is shown in Fig. 2(b). By comparing the surface morphology before and after formation of ZnO layer [see Figs. 2(a) and 2(b)], it was found that the ZnO layer composed of densely interlaced minute crystals was grown uniformly along the irregular surface of the CZTS film lying underneath. Such kind of growth behavior is usually observed in the CVD process when a surface reaction growth mode is dominant.

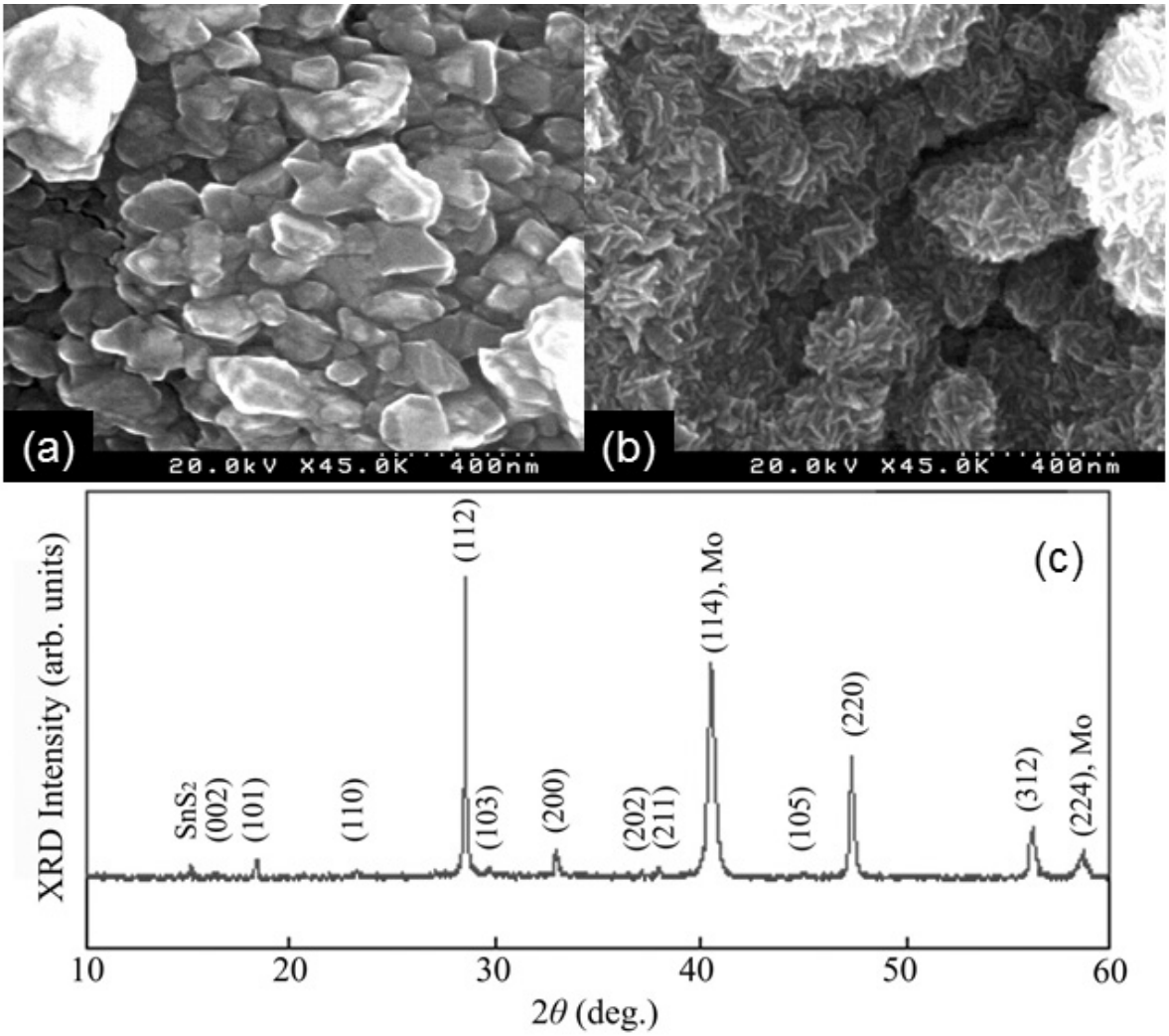

Fig. 2. The surface morphology of CZTS film (a) before, (b) after deposition of ZnO buffer layer. (c) The XRD pattern of CZTS film.

The *J*-*V* characteristics of CZTS/ZnO hetrojunction solar cells prepared at various conditions are shown in Table I. Samples (a), (b), and (c) represented the cells, in which the CZTS/ZnO hetrojunctions were implemented at the deposition temperatures of 400, 350, and 300 ˚C, respectively. The thickness of ZnO buffer layer was set to about 100 nm by adjusting the deposition rate at each growth temperature during USP process. The resistivity of the ZnO buffer layer was increased from 5.6×10^1 to 5.3×10^4 Ω cm as the growth temperature reduced from 400 to 300 ˚C under a constant flow rate of the precursor mist adjusted at 1.4 L/min. Among these three cells, the sample (b) exhibited the highest conversion efficiency (η) of 2.78%, a fill factor (*FF*) of 40%, an open circuit voltage (V_{oc}) of 530 mV, and a short circuit current density (J_{sc}) of 13.0 mA/cm^2. The resistivity of the ZnO layer in the sample (b) was 4.9×10^3 Ω cm. In the case of sample (a) that had the lowest resistivity of 5.6×10^1 Ω cm but preapred at the highest temperature of 400 ˚C, the η was decreased to 1.61%. Similarly, in the sample

(c) that had the highest resistivity of 5.3×10^4 Ω cm but deposited at the lowest temperature of 300 ˚C, the η was decreased to 1.74%. These results indicate that a suitable resistivity of ZnO layer for achieving better solar cell characteristics is in the order of 10^3 Ω cm and the growth temperature not higher than 350 ˚C was preferable. In the other words, it can be said that the deposition of 10^3 Ω cm range ZnO buffer layer at lower temperatures is better to obtain a good CZTS/ZnO hetrojunction.

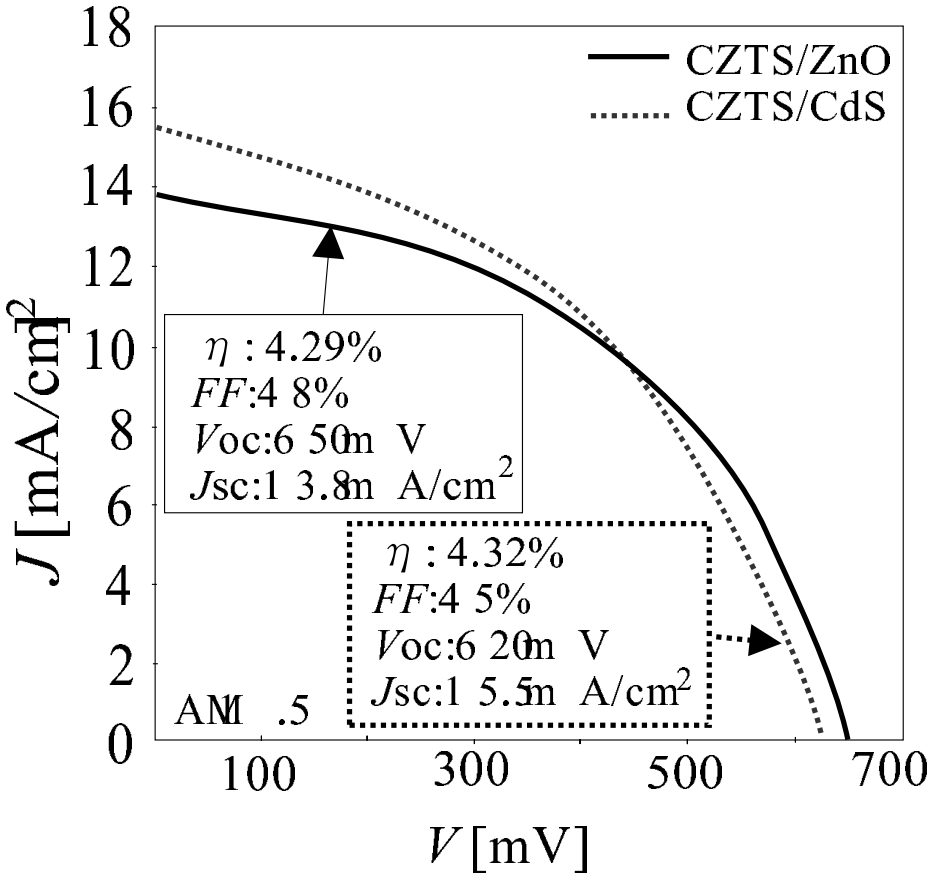

Fig. 3. The *J-V* characteristics of CZTS/ZnO (continuous line) and CZTS/CdS (dashed line) solar cells measured at an effective area of 2.25 mm^2.

In the samples (d) and (e), the CZTS/ZnO hetrojunction was implemented at 300 ˚C under the precursor mist flow rate of 1.0 L/min, and the thickness of deposited ZnO layers was adjusted to about 150 and 200 nm, respectively. Here, the resistivity of each ZnO layer was about 1.4×10^4 Ω cm. Both of the samples (d) and (e) showed the η higher than 2%, which was close to that of the sample (b) prepared at 350 ˚C. Besides, no obvious difference in the characteristics of the two cells was observed due to the change in the thickness of ZnO buffer layers having the same resistivity. In comparing the characteristics of samples (d) and (e) with that of the sample (c) in which the ZnO layer had a resistivity of 5.3×10^4 Ω cm and a thickness of 100 nm, better cell characteristics were achieved in the

samples (d) and (e). Particularly, it is quite obvious that an enhancement of the V_{oc} reaches about 20%. This result suggested that the degradation of cell performance in the sample (c) was mainly due to the increasing of resistivity of ZnO layer nearly by 4 times, although its thickness was thinner than that of the samples (d) and (e). However, in the other samples (not shown in the table) that had ZnO layer with thickness larger than 200 nm but with the same resistivity to the sample (c), rapid deterioration of the cell characteristics was observed. It may be considered that beyond 200 nm thickness, the ZnO layer contributes as a series resistance, giving rise to deterioration of the short circuit current and cell performance consequently.

In order to obtain a suitable CZTS/ZnO hetrojunction for optimizing the cell performance, a ZnO layer with a thickness of about 60 nm and a resistivity in the 10^3 Ω cm range was deposited on the CZTS film at 300 ˚C under precursor mist flow rate of 0.8 L/min. In this optimized sample, a V_{oc} of 650 mV has been achieved, resulting in the best η of 4.29%, FF of 48%,and J_{sc} of 13.8 mA/cm^2 as shown in Fig. 3 (see continuous line). There was no improvement in the performance of cells with ZnO buffer layer thickness of about 60 nm, where the CZTS/ZnO junctions were fabricated at the temperatures higher than 300 ˚C (data not shown). This could be due to the degradation of CZTS absorber layer caused by the thermal diffusion at the deposition temperatures of ZnO layer higher than 300 ˚C. To conclude above, it may be considered that the optimum junction formation temperature is near 300 ˚C to obtain 10^3 Ω cm range resistivity and an optimum thickness of ZnO buffer layer is about 60 nm.

Table I. Characteristics of CZTS/ZnO solar cells prepared under various conditions.

Sample	ZnO buffer Layer				η	FF	V_{oc}	J_{sc}
	Growth temperature (˚C)	Mist flow rate (L/min)	Thickness (nm)	Resistivity (Ω cm)	(%)	(%)	(mV)	(mA/cm^2)
(a)	400	1.4	100	5.6×10^1	1.61	32	450	11.1
(b)	350	1.4	100	4.9×10^3	2.78	40	530	13.0
(c)	300	1.4	100	5.3×10^4	1.74	35	440	11.5
(d)	300	1.0	150	1.4×10^4	2.31	39	530	11.2
(e)	300	1.0	200	1.4×10^4	2.54	39	535	12.1

3.2 Comparison of CZTS/ZnO and CZTS/CdS cells

A comparison of the J-V characteristics of the optimized CZTS/ZnO and the conventional CZTS/CdS solar cells measured at an effective area of 2.25 mm^2 were shown in Fig. 3. The J_{sc} of the CZTS/ZnO

and CZTS/CdS cells was 13.8 and 15.5 mA/cm^2, while the V_{oc} was 650 and 620 mV, respectively. In the CZTS/ZnO cell, the V_{oc} was enhanced by 5%, which was a trade off due to the decrease of J_{sc} by 12%: there was no obvious improvement in the η: 4.29% and *FF*: 48% when compared with that of the CZTS/CdS cell (η: 4.32% and *FF*: 45%). The achievement of larger V_{oc} in the CZTS/ZnO cell could be considered as a benefit of utilizing wider band gap ZnO that might induce the formation of a higher built-in potential. On the other hand, the decrease of J_{sc} could be related with the recombination of minority carriers that is enhanced by the defects at CZTS/ZnO interface.

The experimental data of *QE* for the two cells was compared in Fig. 4. As can be seen clearly from the curves shown here, the *QE* was gradually improved as the wavelength of photons became shorter than 510 nm. However, in the region of wavelength longer than 510 nm, almost similar response to that of the conventional CZTS/CdS cell was found. This transition wavelength at 510 nm is in consistency with that of the absorption edge of CdS. Hence, such an improvement at the wavelength regions shorter than 510 nm could be considered mainly due to the increase of transparency by utilizing a wider band gap ZnO buffer layer because the absorption of incident short-wavelength photons was increased, resulting in an enhancement of the *QE*. In the case of the CdS buffer layer, to the contrary, the shorter wavelength photons beyond this absorption edge of 510 nm would be considerably decayed before reaching the p-n junction lying beneath.

To investigate the in-plane uniformity of the solar cells, the characteristics of CZTS/ZnO and CZTS/CdS cells were evaluated at two different types of surface area. A smaller area cell was 1.5×1.5 mm^2 in effective size, and the larger one was 5.0×5.0 mm^2, respectively. The result shown in Table II clearly shows that there is no deterioration in the *J-V* characteristics of the CZTS/ZnO cell when the effective surface area of the cell is increased. However, a marked decrease in V_{oc} as well as the η and *FF* are observed in the case of conventional CZTS/CdS cell. According to this result we may consider that the use of the ZnO buffer layer deposited by USP is favorable to realize a uniform coating on the substrates having the irregular surface morphologies or acute geometries [see Fig. 2(b) as well as Fig. 5], since the growth mechanism for the ZnO film is based on the surface reaction which does not damage the substrate. In contrast to this, the deposition mechanism of CBD films is based on the precipitation in a precursor solution rather than surface reaction so that the thickness of precipitates is more likely to vary at the irregular surface of the substrates, especially when there is an acute geometry. A cross sectional TEM image and a Z-contrast (ZC) image of the CZTS/ZnO cell were shown in Figs. 5(a) and 5(b), respectively. It is found from the images that the interface between CZTS and ZnO is continuous and no voids are observed even at the acute junction morphology, indicating that the USP growth process of ZnO layer is suitable for the fabrication of heterojunction on the CZTS film with irregular geometries. However, the grain size of the CZTS film was quite small and several voids were

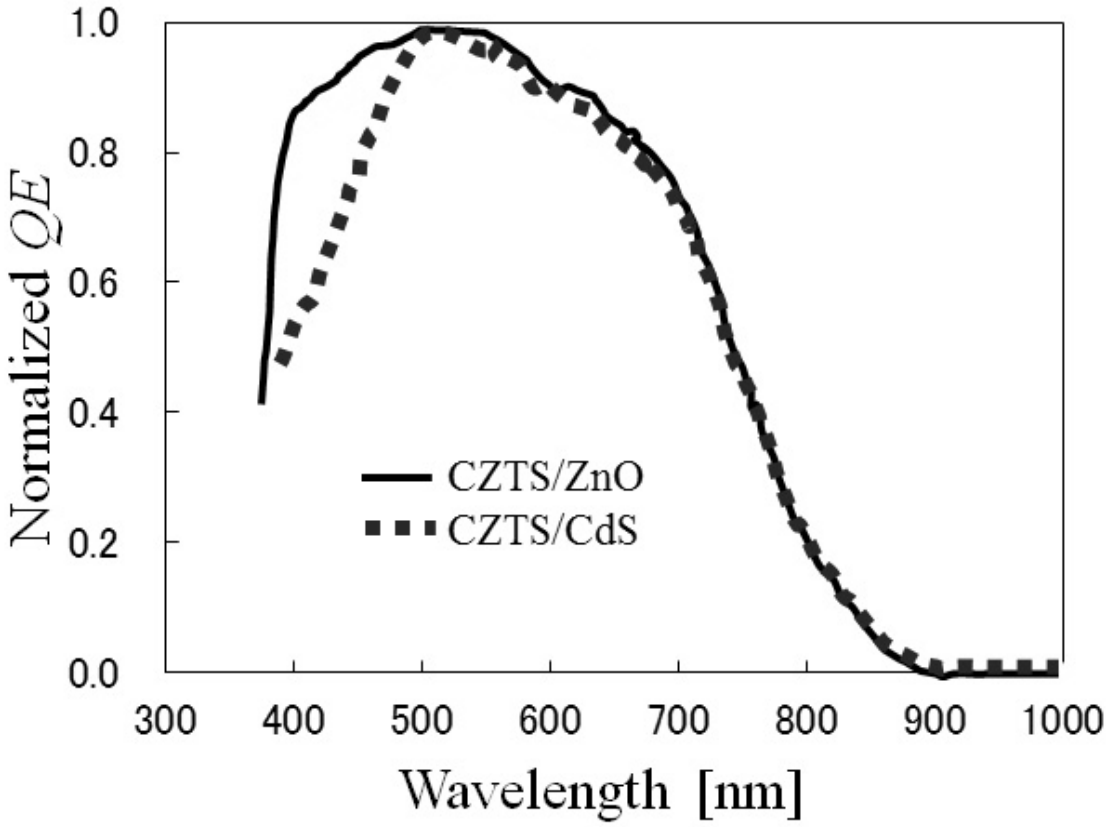

Fig. 4. The *QE* of CZTS/ZnO (continuous line) and CZTS/CdS (dashed line) solar cells.

located at the interface of the CZTS film and Mo back electrode. The voids were identified clearly as the white spots in the CZTS layer shown in Fig. 5(a) and also as the dark spots in the ZC image of Fig. 5(b). The existence of the voids in CZTS layer could be the main reason why the J_{sc} of the cells deteriorates. In order to realize a high performance CZTS solar cell, a high quality single phase CZTS absorber film with no voids will be needed.

Table II. Characteristics of CZTS/ZnO and CZTS/CdS solar cells with different surface area.

	CZTS/ZnO		CZTS/CdS	
	2.25 mm^2	25 mm^2	2.25 mm^2	25 mm^2
η (%)	2.96	3.08	2.57	0.61
FF (%)	46	46	43	27
V_{oc} (mV)	513	550	473	205
J_{sc} (mA/cm^2)	12.5	12.2	12.6	10.9

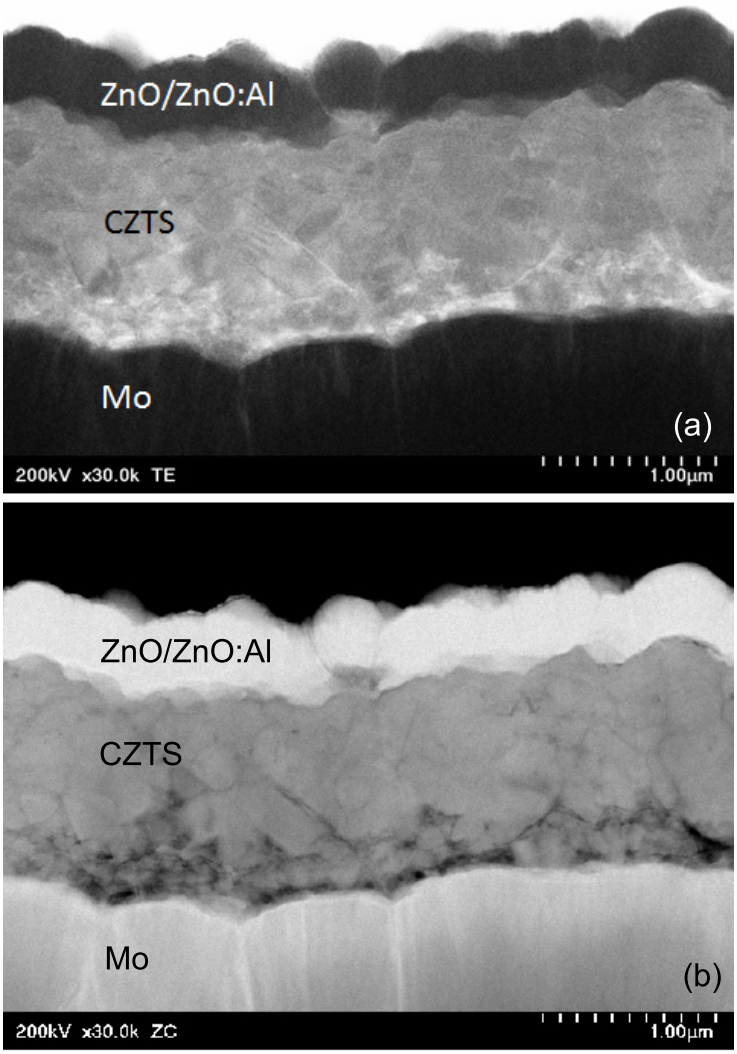

Fig. 5. Cross sectional (a) TEM image and (b) Z-contrast image of CZTS/ZnO solar cell.

4. Conclusions

A CZTS absorber layer was prepared from the laminated metallic precursor which was annealed under ambient of elemental sulfur vapor. The sulfurization was performed in a closed glass tube heated with an infrared furnace. The conversion efficiency over 4% was achieved by utilizing this CZTS film. There was a SnS_2 impurity phase in CZTS films as well as several voids near the surface of a Mo back electrode. We have confirmed that the performance of CZTS/ZnO cell was not inferior to that of the conventional CZTS/CdS cell. Therefore it is possible to replace a toxic CdS buffer layer with the environment-friendly ZnO buffer layer. By utilizing wider band gap ZnO instead of toxic CdS, an improvement in the open circuit voltage was achieved. Besides, the relative quantum efficiency in the wavelength regions shorter than 510 nm was also enhanced. The in-plane uniformity of CZTS/ZnO

solar cell was improved by depositing the ZnO layer via ultrasonic spray pyrolysis.

Acknowledgments

Special thanks are due to Mr. Isamu Minemura for many help with the construction of experimental apparatus and Mr. Tomohiko Yamakami for TEM photography.

References

1) K. Ito and T. Nakazawa: Jpn. J. Appl. Phys. **27** (1988) 2094.
2) K. Ito and T. Nakazawa: Proc. 4th Int. Conf. Photovoltaic Science and Engineering, 1989, p. 341.
3) N. Nakayama and K. Ito: Appl. Surf. Sci. **92** (1996) 171.
4) M. Altosaar, J. Raudoja, K. Timmo, M. Danilson, M. Grossberg, J. Krustok, and E. Mellikov: Phys. Status Solidi A **205** (2008) 167.
5) T. K. Todorov, K. B. Reuter, and David B. Mitzi: Adv. Mater. **22** (2010) E156.
6) M. A. Green, K. Emery, Y. Hishikawa, and W. Warta: Prog. Photovoltaics **17** (2009) 85.
7) D. Butler: Nature **454** (2008) 558.
8) G. Zoppi, I. Forbes, R. W. Miles, P. J. Dale, J. J. Scragg, and L. M. Peter: Prog. Photovoltaics **17** (2009) 315.
9) H. Katagiri, K. Jimbo, W. S. Maw, K. Oishi, M. Yamazaki, H. Araki, and A. Takeuchi: Thin Solid Films **517** (2009) 2455.
10) H. Katagiri, K. Jimbo, S. Yamada, T. Kamimura, W. S. Maw, T. Fukano, T. Ito, and T. Motohiro: Appl. Phys. Express **1** (2008) 041201.
11) H. Katagiri, K. Jimbo, R. Kimura, T. Kamimura, S. Yamada, W.S. Maw, H. Araki, and K. Oishi: Thin Solid Films **515** (2007) 5997.
12) S. Chen, X. G. Gong, A. Walsh, and S. H. Wei: Appl. Phys. Lett. **96** (2010) 021902.
13) S. Chen, J. H. Yang, X. G. Gong, A. Walsh, and S. H. Wei: Phys. Rev. B **81** (2010) 245204.
14) R. Schurr, A. Hölzing, S. Jost, R. Hock, T. Voβ, J. Schulze, A. Kirbs, A. Ennaoui, M. Lux-Steiner, A. Weber, I. Kötschau, and H.-W. Schock: Thin Solid Films **517** (2009) 2465.
15) A. Ennaoui, M. Lux-Steiner, A. Weber, D. Abou-Ras, I. Kötschau, H. W. Schock, R. Schurr, A. Hölzing, S. Jost, R. Hock, T. Voβ, J. Schulze, and A. Kirbs: Thin Solid Films **517** (2009) 2511.
16) M. T. Htay, Y. Hashimoto, and K. Ito: Jpn. J. Appl. Phys. **46** (2007) 440.
17) N. Izyumskaya, V. Avrutin, Ü. Özgür, Y. I. Alivov, and H. Morkoç: Phys. Status Solldi B **244** (2007) 1439.
18) C. Kittel: *Introduction to Solid State Physics* (Wiley, New York, 2005) 8th ed., p. 190.
19) N. Momose, M. T. Htay, T. Yudasaka, S. Igarashi, T. Seki, S. Iwano, Y. Hashimoto, and K. Ito: to be published in Jpn. J. Appl. Phys.